NASA TECHNICAL MEMORANDUM

NASA TM X-3485

NASA TM X-3485

A HEAVY ION BEAM PROBE SYSTEM FOR INVESTIGATION OF A MODIFIED PENNING DISCHARGE

George X. Kambic and Walter M. Krawczonek

Lewis Research Center

Cleveland, Ohio 44135

NATIONAL AERONAUTICS AND SPACE ADMINISTRATION • WASHINGTON, D. C. • MARCH 1977

1. Report No.	2. Government Accession No.	3. Recipient's Catalog No.
NASA TM X-3485		

4. Title and Subtitle	5. Report Date
A HEAVY ION BEAM PROBE SYSTEM FOR INVESTIGATION OF A MODIFIED PENNING DISCHARGE	March 1977
	6. Performing Organization Code

7. Author(s)	8. Performing Organization Report No.
George X. Kambic and Walter M. Krawczonek	E-8869
	10. Work Unit No.
9. Performing Organization Name and Address	506-25
Lewis Research Center National Aeronautics and Space Administration Cleveland, Ohio 44135	11. Contract or Grant No.
	13. Type of Report and Period Covered
12. Sponsoring Agency Name and Address	Technical Memorandum
National Aeronautics and Space Administration Washington, D. C. 20546	14. Sponsoring Agency Code

15. Supplementary Notes

16. Abstract

An ion beam probe diagnostic system can measure time- and space-resolved profiles of plasma space potential and electron density. In combination with a computer iterative technique, the ion beam probe can determine both the space potential profile in plasmas containing strong electric fields and potentials comparable in magnitude to the energy of the probing ion beam. During ion beam probing of a modified Penning discharge, several groups of secondary ions have been observed coming from the plasma with a fixed primary-beam energy and momentum. The energies of these ions were within 10 percent of the values predicted by a computer-generated model of the potential profile in the plasma. The mechanical and electronic components of the system are described, with particular emphasis on those features required to probe plasma potentials comparable in magnitude to the ion beam energy.

17. Key Words (Suggested by Author(s))	18. Distribution Statement
Penning discharge; Potential fields; Potential gradients; Ion beam probing; Ion beam probe	Unclassified - unlimited STAR Category 75

19. Security Classif. (of this report)	20. Security Classif. (of this page)	21. No. of Pages	22. Price*
Unclassified	Unclassified	33	A03

* For sale by the National Technical Information Service, Springfield, Virginia 22161

A HEAVY ION BEAM PROBE SYSTEM FOR INVESTIGATION OF A MODIFIED PENNING DISCHARGE

by George X. Kambic* and Walter M. Krawczonek

Lewis Research Center

SUMMARY

An ion beam probe diagnostic system can measure time- and space-resolved profiles of plasma space potential and electron density. In combination with a computer iterative technique, the ion beam probe can determine both the space potential profile in plasmas containing strong electric fields and potentials comparable in magnitude to the energy of the probing ion beam. During ion beam probing of a modified Penning discharge, several groups of secondary ions have been observed coming from the plasma with a fixed primary-beam energy and momentum. The energies of these ions were within 10 percent of the values predicted by a computer-generated model of the potential profile in the plasma. The mechanical and electronic components of the system are described, with particular emphasis on those features required to probe plasma potentials comparable in magnitude to the ion beam energy.

INTRODUCTION

The heavy ion beam probe (refs. 1 and 2) is a nonperturbing plasma diagnostic. It has the unique ability to measure plasma space potential directly. For this reason, it is important to develop this diagnostic for the investigation of laboratory-scale and fusion-related plasmas containing strong electric fields (ref. 3). It can make time- and space-resolved measurements of electron density, electron temperature, plasma potential, and axial current density (refs. 4 to 6). Interest in this diagnostic method at

*National Research Council - National Aeronautics and Space Administration Research Associate.

Lewis stems from the existence of plasmas containing strong electric fields in their interiors. These devices include the modified Penning discharge (refs. 7 and 8) and the bumpy torus (refs. 9 and 10). This report describes the mechanical and electronic systems required to implement ion beam probing on the modified Penning discharge.

The probe built at Lewis is based on the ion beam probing technique developed by Hickok and Jobes (refs. 4 and 5). Figure 1 illustrates the principle of the ion beam probe. A monoenergetic ion beam (I^+) is injected into a plasma confined by an axial magnetic field. A fraction of this primary beam, called the secondary beam, is doubly

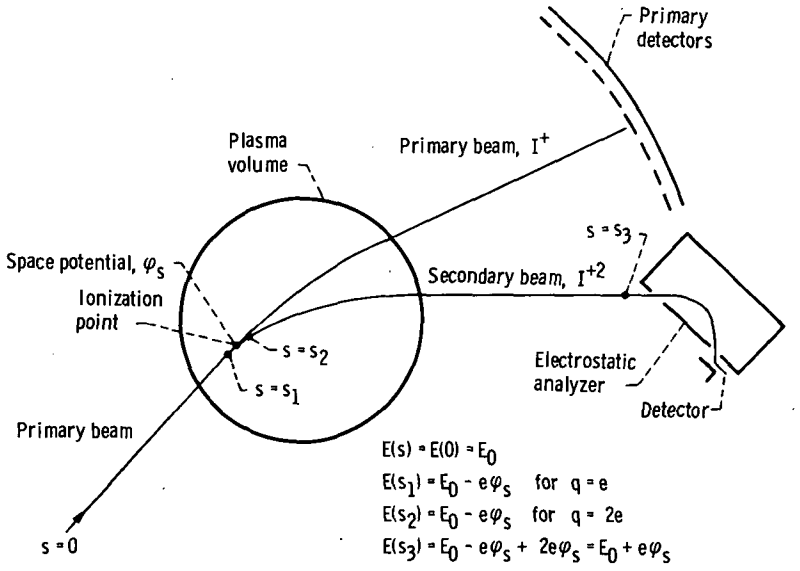

Figure 1. - Principle of ion beam probing spatial resolution and space potential measurement.

ionized and magnetically separated from the primary beam and is detected outside the plasma volume. Secondary ions are generated along the length of the primary-beam path through the plasma, but a given detector sees only those generated in a small volume of the plasma. By measuring the properties of the secondary beam, including energy, current, and momentum, the previously listed plasma characteristics can be determined. In this report, we concentrate on measuring the plasma potential profile. The potential is determined by calculating the energy of an ion as it passes through the plasma. The ion has an initial energy E_0 at $s = 0$, where s is the length along the beam path:

$$E(s)\big|_{s=0} = E(0) = E_0 \tag{1}$$

As the ion penetrates the plasma, it changes total energy as determined by the space potential φ_s:

$$E(s_1) = E_0 - e\varphi_s \tag{2}$$

If the ion is then ionized to a +2 state, the final secondary-ion energy is equal to the initial primary-ion energy plus the plasma space potential, as given in equation (3).

$$E(s_3) = E_{final} \tag{3a}$$

$$E(s_3) = E_0 - e\varphi_s + 2e\varphi_s \tag{3b}$$

$$E(s_3) = E_0 + e\varphi_s \tag{3c}$$

In previous ion beam probing, plasma potentials have been about 10^{-2} to 10^{-3} times the primary-ion-beam energy, $e\varphi \ll E_i$. In the modified Penning discharge plasma, the potential can be many kilovolts (ref. 8). With the Lewis probe, we measure potentials that are large fractions, 0.25 to 0.50, of the primary-ion-beam energy.

The Lewis ion beam probe uses a monoenergetic beam of thallium ions (Tl^+). The beam is injected into the midplane of the modified Penning discharge, which is sustained by a pair of Penning anode rings. The maximum magnetic field used was 0.46 tesla. For a thallium ion (mass, 204.4 atomic mass units) of 20-keV energy, the ion trajectories through the magnetic and electric fields of the plasma cannot be approximated by a simple trajectory appropriate to motion in the magnetic field alone. If the maximum potential in the plasma is of the order of the anode voltage, the secondary-ion energy can change by 50 percent. Since the ion trajectories are no longer uniquely known, spatial resolution is lost.

This problem was dealt with by using a computer program to calculate a self-consistent model of a plasma potential profile. In its simplest form, it solves the equations of motion of a particle of mass m and charge q in electric and magnetic fields:

$$m\ddot{\vec{x}} = q(\vec{E} + \dot{\vec{x}} \times \vec{B}) \tag{4}$$

The magnetic field is known everywhere and the electric field is obtained by differentiation of the potential profile. This calculation is described in more detail elsewhere (ref. 11). The shape of the potential is varied in an iterative manner until measured and calculated trajectories are in agreement.

ION BEAM PROBE APPARATUS

The Lewis ion beam probe uses a thallium ion beam with energies of 15 to 40 keV. The modified Penning discharge facility is shown in figure 2. The beam is injected into

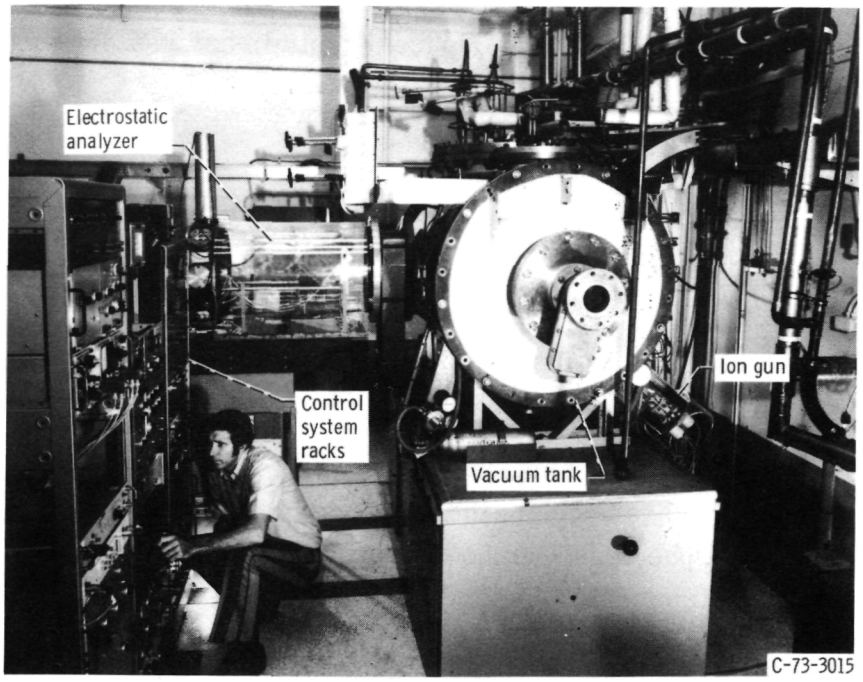

Figure 2. - NASA Lewis modified Penning discharge and ion beam probe facility.

the midplane of the mirror magnetic field of the modified Penning discharge. The large vacuum tank contains the Penning anode rings and the magnetic field coils. A cutaway drawing of the plasma region is shown in figure 3. The Penning anode rings are shown, along with the grounded cylindrical wire mesh that surrounds the plasma and symmetrizes the radial potential in the midplane of the system. Figure 4 shows the screen, the anode support shaft, and one of the two superconducting coils. The plasma is confined to the region inside the anode rings. The ion beam passes between the double anode rings perpendicular to the magnetic field. The primary beam is detected with either the electrostatic analyzer or the primary detector, and the secondary beam is detected with the electrostatic analyzer.

Figure 5 is a schematic of the various components of the plasma and probe system; it shows the ion gun, the anode ring, the grounded screen, the electrostatic analyzer, and the primary detector. The primary detector is a set of 33 flat Langmuir probes

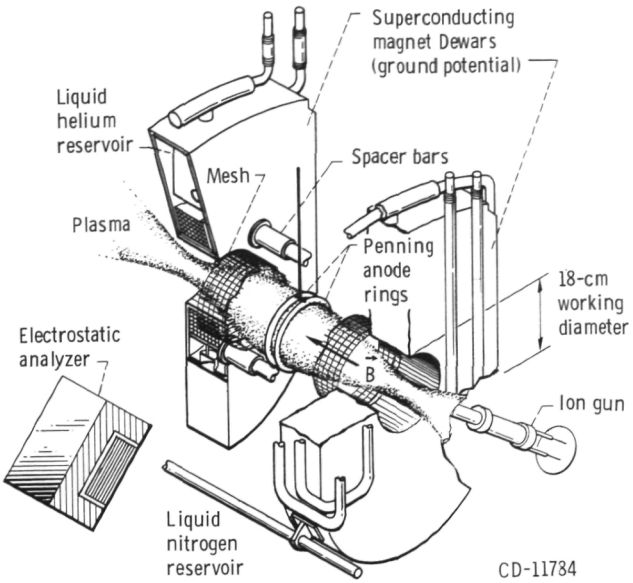

Figure 3. - Cutaway drawing of apparatus.

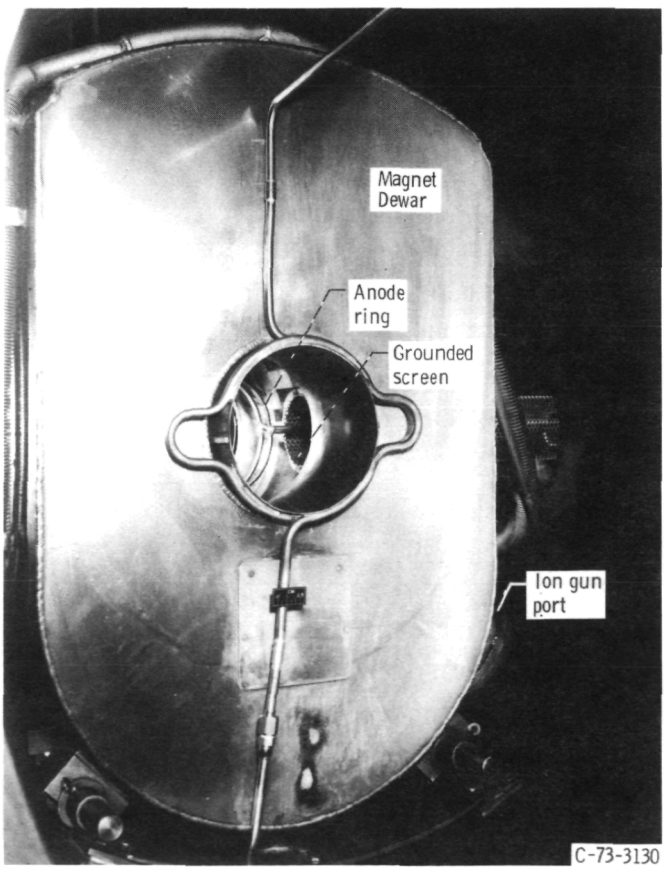

Figure 4. - Magnet Dewar, anode ring, and grounded screen.

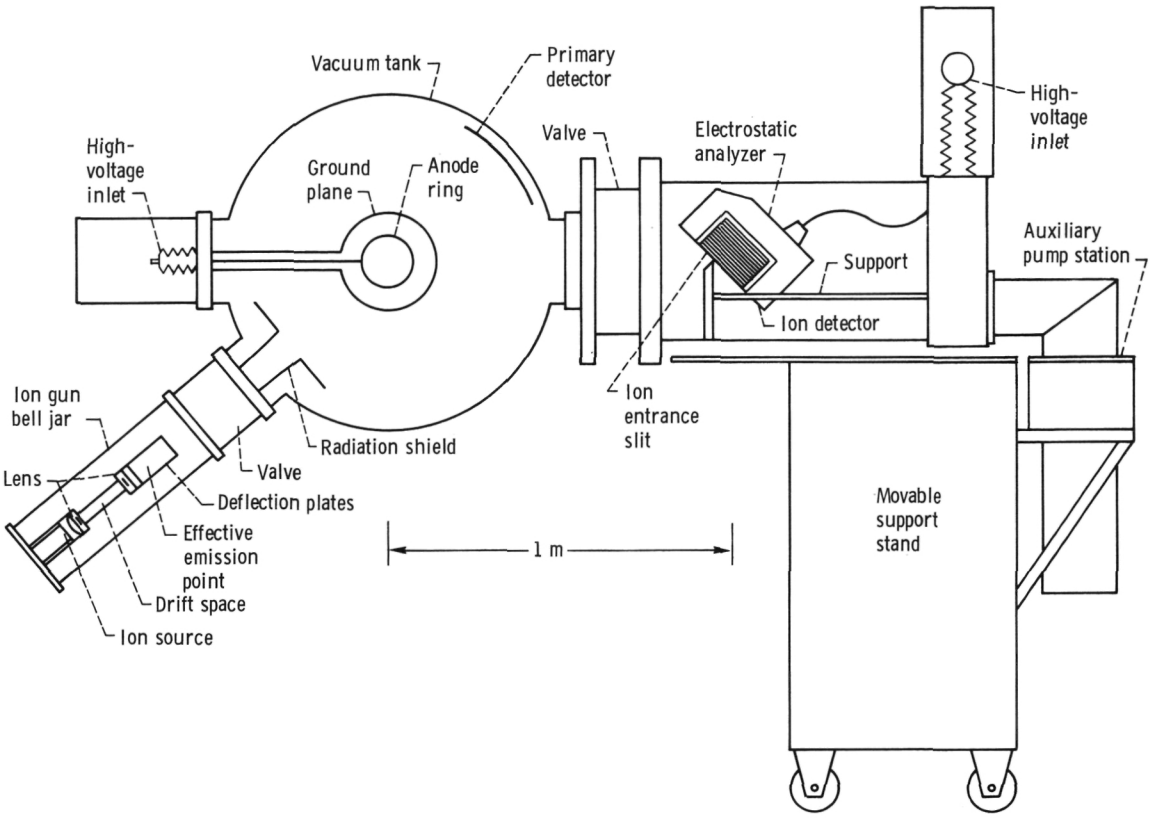

Figure 5. - Schematic of ion beam probe system.

placed on the tank wall in the path of the primary beam. The overall deflection angle of the beam going into the electrostatic analyzer is 40^{o}. The maximum midplane magnetic field of which the coil system is capable is 0.8 tesla, but studies were done at a constant 0.46 tesla. Since the scaling of the ion beam can be expressed as $E_i m_i \propto B^2 r^2$, the beam probe characteristics of other systems can be scaled from the characteristics of this system.

The ion gun used is shown in figure 6(a). It is basically the same gun used by Hickok and Jobes (ref. 5). It uses Pierce extraction electrodes near the ion source (ref. 12). It is operated by means of a resistive divider string and keeps the beam full width at half maximum to within 0.5 centimeter over the beam energy range used. The optimum voltage ratios for the electrodes of the gun were found by trial and error. The gun is dependable and convenient in operation.

The thallium ion source is a thallium zeolite packed into the top of a 0.64-centimeter-diameter ceramic tube, shown in figure 6(b). The tube has an 0.5-centimeter-diameter insert that is inset 0.64 centimeter. A 0.025-centimeter-diameter

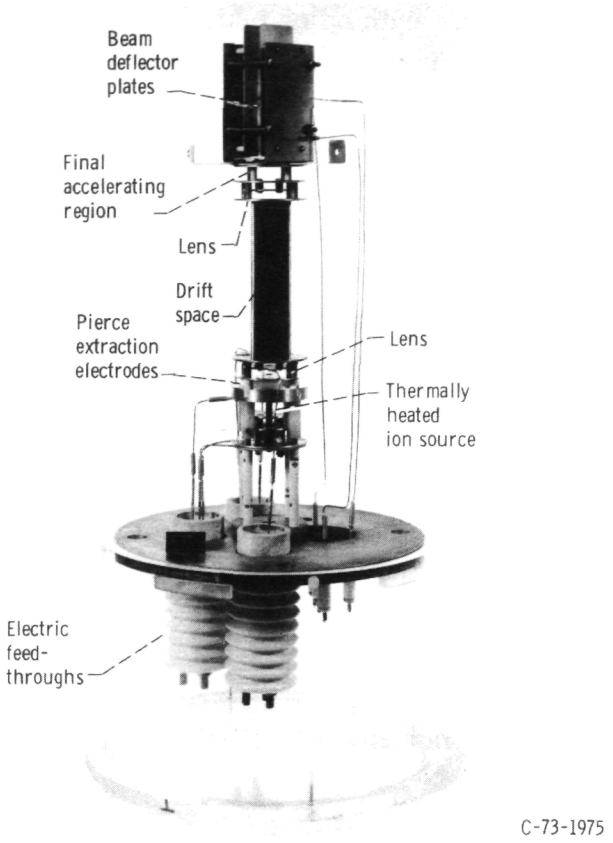

(a) Overall view.

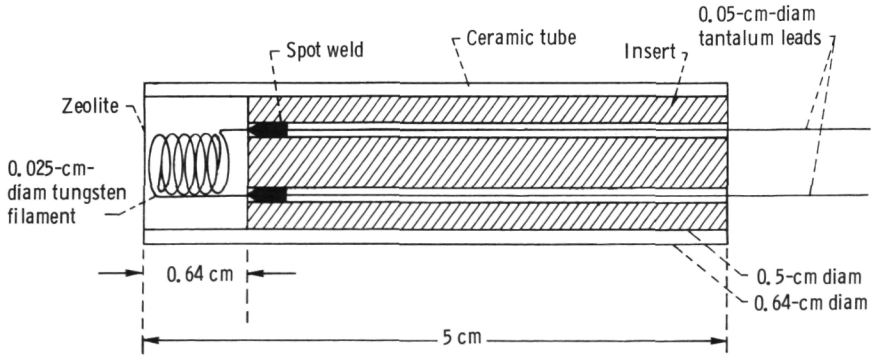

(b) Details of thallium ion source.

Figure 6. - Electrostatic ion gun.

tungsten filament is placed in the well at the top of the ceramic tube for thermionic heating of the zeolite. Tantalum leads 0.05 centimeter in diameter are welded to the tungsten filament. The sources were run for 40 to 50 hours at constant beam current. The zeolite material can be doped with other materials such as sodium or lithium.

The electrostatic energy analyzer is a parallel-plate, energy selection system that operates around a mean entrance angle of 45° and a geometric gain of 1 (refs. 13 to 15). At this angle, the voltage across the analyzer in volts is numerically equal to the energy of a doubly charged secondary ion in electron volts when the height of the analyzer is equal to the separation of the ion entrance and exit slits. A diagram of the analyzer is shown in figure 7. This analyzer is sensitive to small changes in the beam energy. It was useful in detecting an 8-volt oscillation in the ion gun power supply when the primary-ion energy E_i was 6 keV. At this time the analyzer was detecting primary ions so the voltage across the analyzer V_{ea} was 12 keV. Although the system can measure small changes in beam energy, we used it to measure plasma potentials that were many kilovolts.

The location of the electrostatic analyzer shown in figure 5 was chosen on the basis of calculated ion trajectories. These trajectories took into account a potential profile based on a model for the modified Penning discharge developed by Roth (ref. 8). The split-plate detector of the +2 ions can operate as an infinitely thin line detector when used in conjunction with a feedback amplifier. The feedback circuit is part of the electronic system for the probe. The associated electronic system is shown in a block dia-

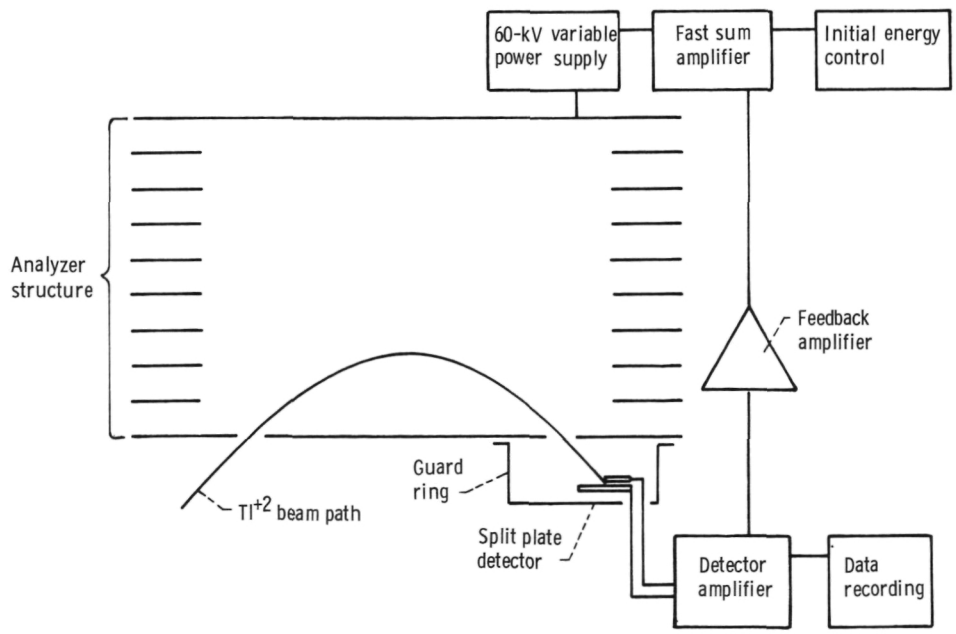

Figure 7. - Electrostatic energy analyzer and feedback loop.

gram in figure 8(a) and in schematic form in figure 8(b). One innovation in this system is the use of separate high-voltage power supplies to operate the ion gun and the analyzer, a result of the high space potentials existing in the plasma.

The electronic system comprises (1) the scan control and variable-time-base generator, (2) the initial value sets (for the energies and sweep angles) and scaling (for the ion mass and magnetic field), (3) the feedback circuitry and beam detection, and (4) data acquisition.

One function of the electronic system is to control the primary-ion-beam energy and injection angle into the plasma. The initial ion gun energy can be set, and the magnitude of the magnetic field can be scaled. The secondary beam is detected in the split-plate detector and amplified in a fast amplifier. The feedback amplifier for the detection system serves to focus the secondary ions onto the detector by varying the voltage across the analyzer. In a plasma where the space potential is small compared with the ion energy, this double power supply arrangement is unnecessary and the plasma potential can be measured in the manner described in references 1 and 2.

The scan control and variable-time-base generator starts and stops beam sweeps through the plasma, sets the number of ionization points that are to be measured, and controls the length of time the primary beam stays at each ionization point. The timing

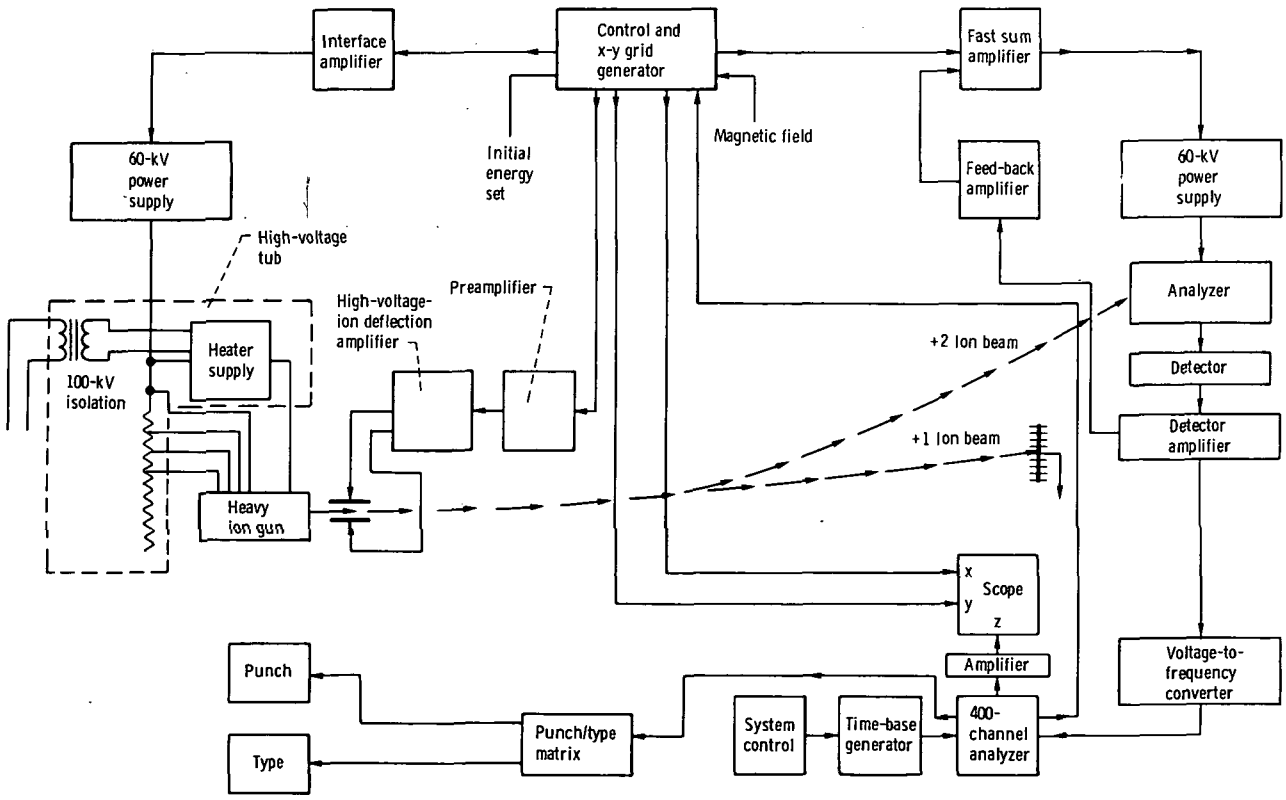

(a) Block diagram.

Figure 8. - Electronic system associated with feedback circuit.

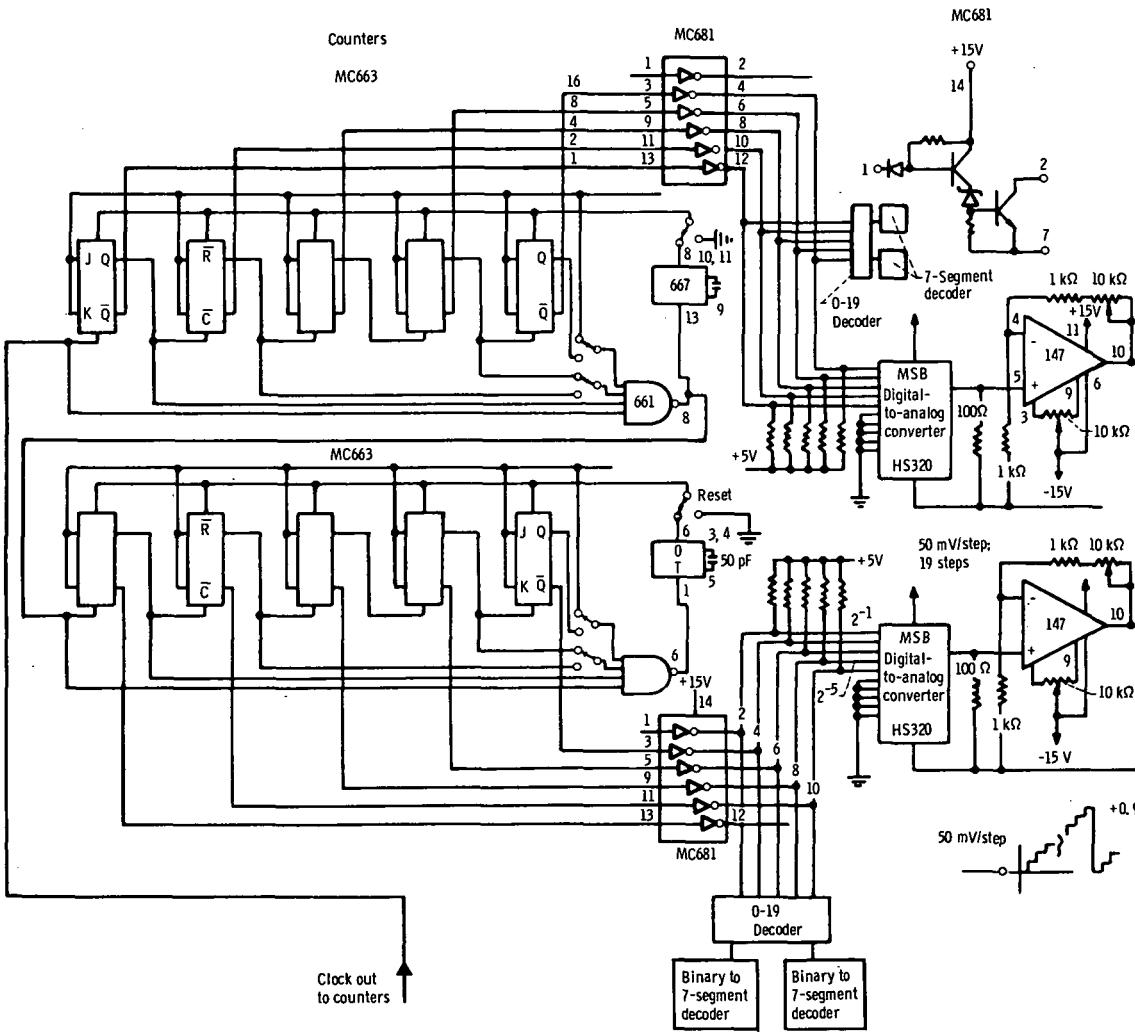

(b) Wiring diagram.

Figure 8. - Continue

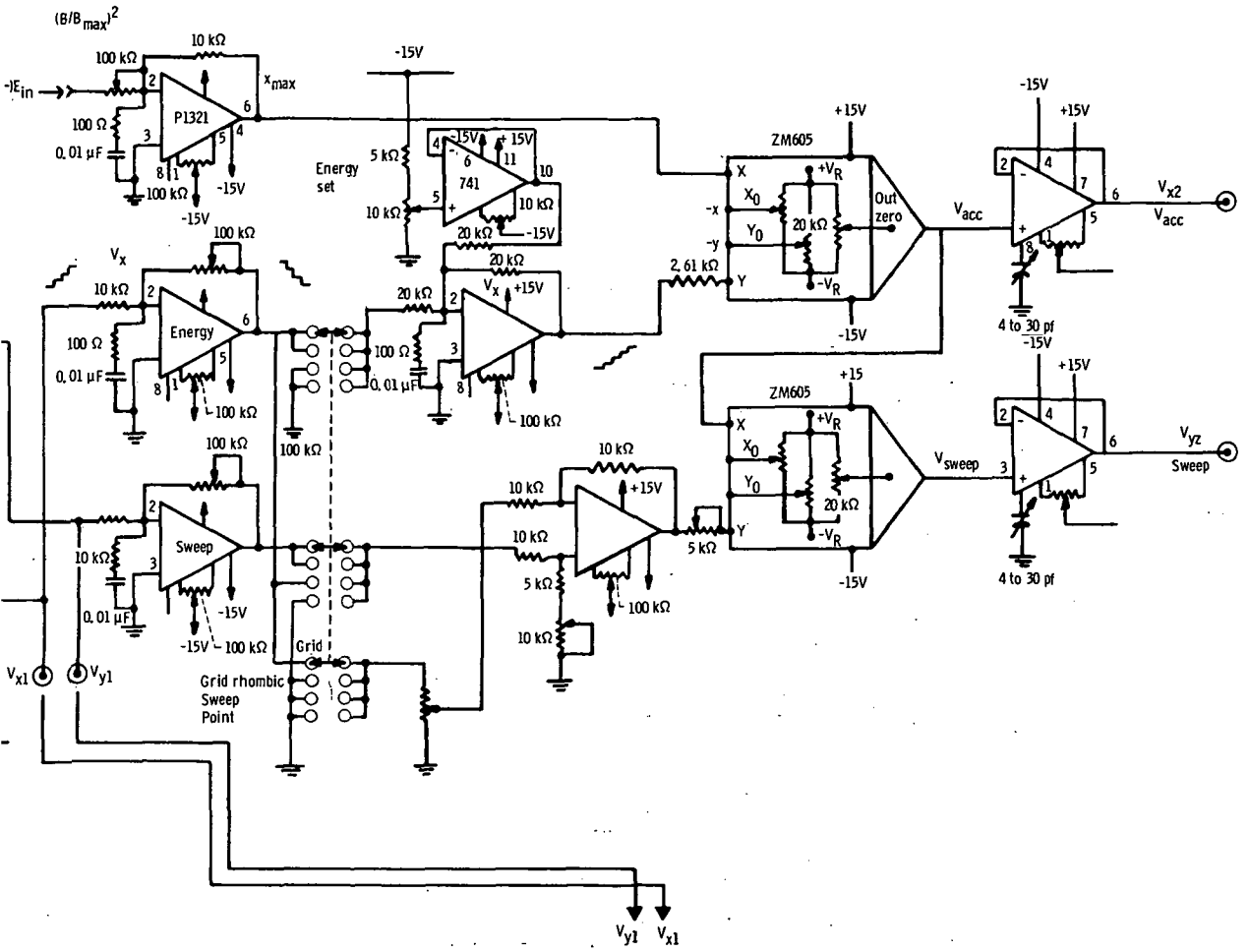
$(B/B_{max})^2$
$-E_{in}$
100 kΩ
10 kΩ
P1321
x_{max}
100 Ω
0.01 μF
100 kΩ
-15V
Energy set
5 kΩ
10 kΩ
741
20 kΩ
+15V
ZM605
X
X_0
-x
Y_0
-y
Y
$+V_R$
$-V_R$
Out zero
2.61 kΩ
V_{acc}
4 to 30 pf
V_{x2}
V_x
Energy
Sweep
V_{sweep}
V_{yz}
Grid
Grid rhombic Sweep Point
V_{x1}
V_{y1}

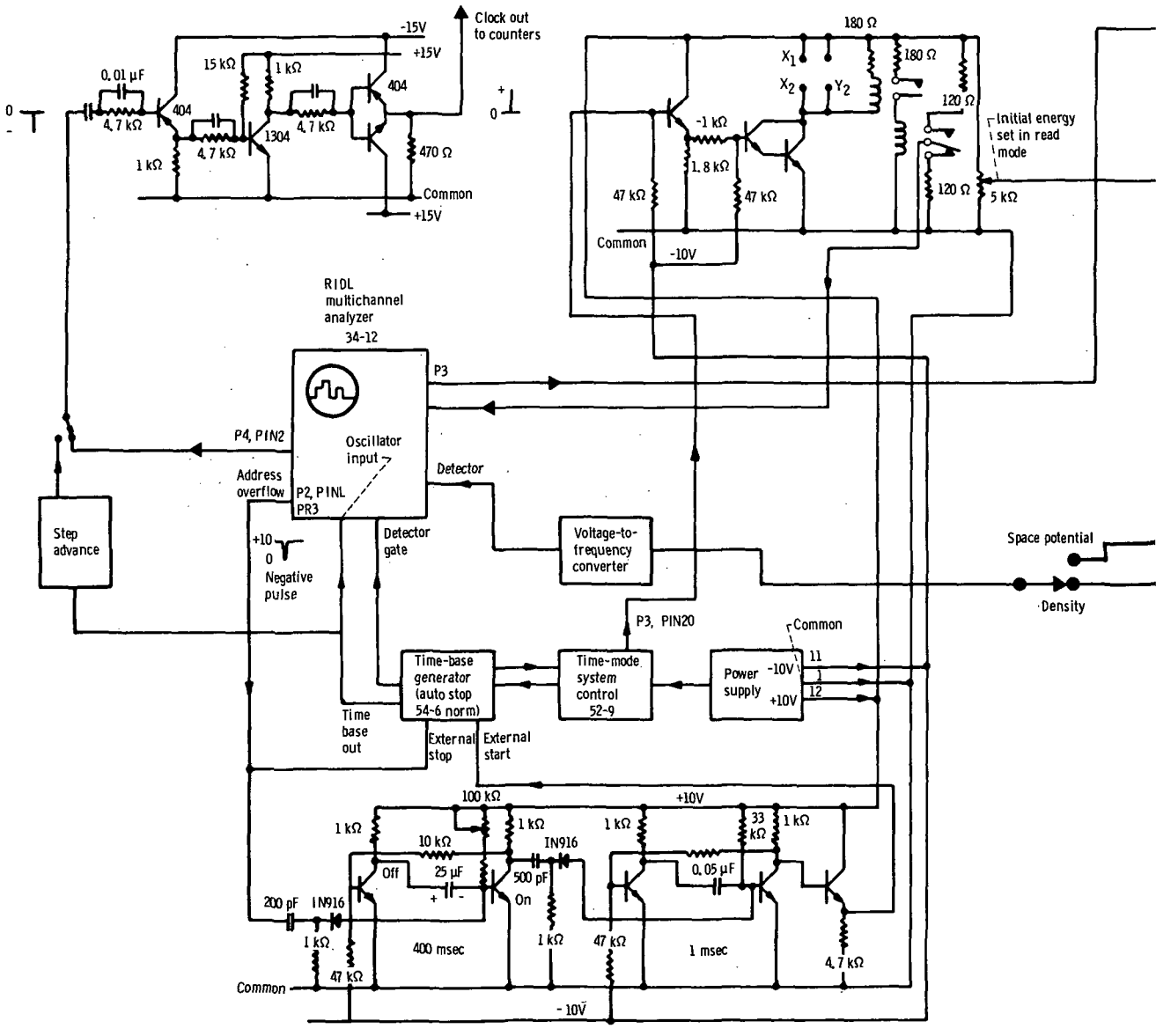

(b) Continued.

Figure 8. - Continued.

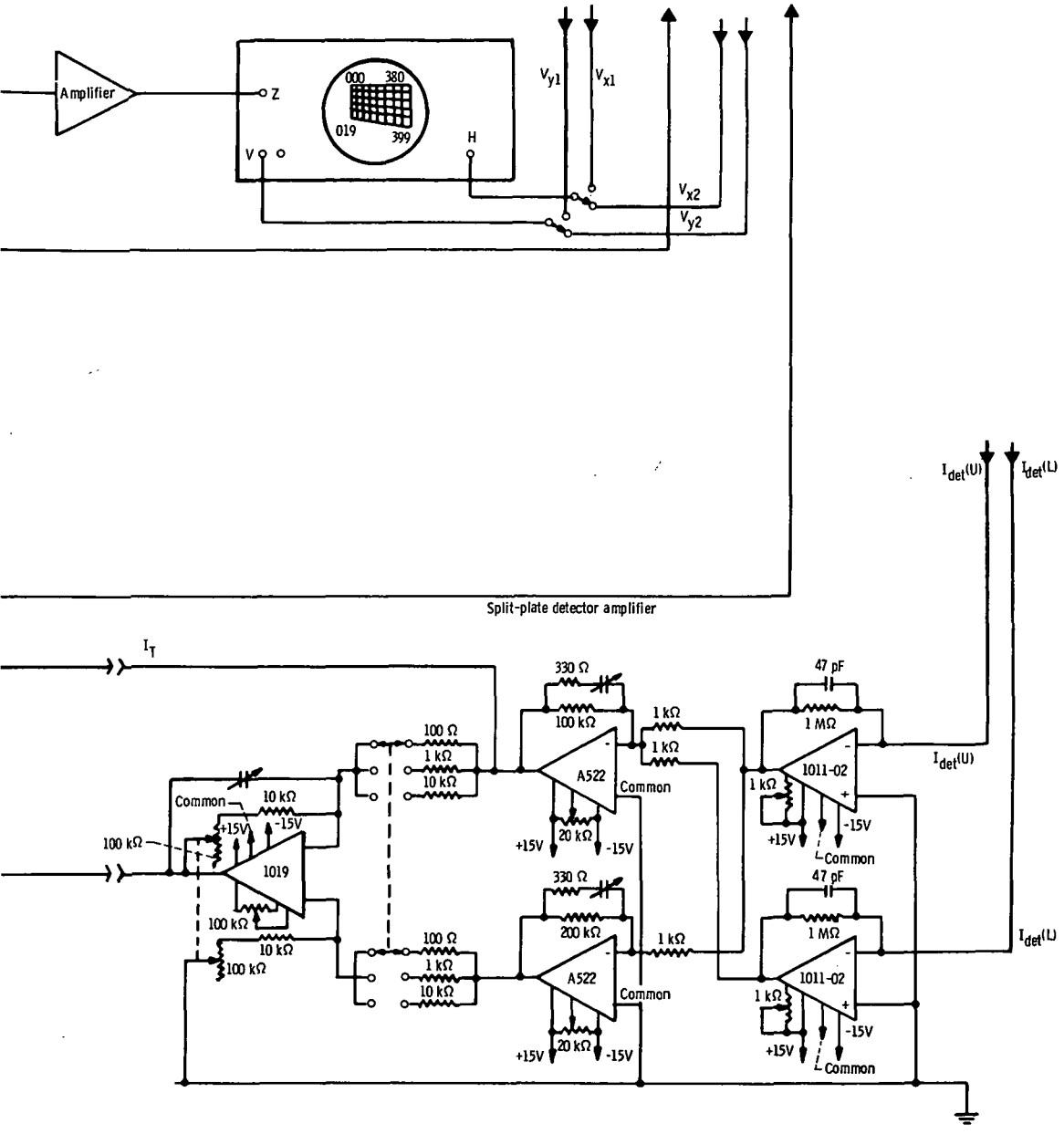
Amplifier
Z
V
H
000
380
019
399
V_{y1}
V_{x1}
V_{x2}
V_{y2}
$I_{det}(U)$
$I_{det}(L)$
Split-plate detector amplifier
I_T
100 kΩ
Common
10 kΩ
+15V
-15V
1019
100 kΩ
10 kΩ
100 kΩ
100 Ω
1 kΩ
10 kΩ
330 Ω
100 kΩ
A522
Common
+15V
20 kΩ
-15V
1 kΩ
1 kΩ
47 pF
1 MΩ
1011-02
1 kΩ
+15V
-15V
Common
330 Ω
200 kΩ
A522
Common
+15V
20 kΩ
-15V
1 kΩ
47 pF
1 MΩ
1011-02
1 kΩ
+15V
-15V
Common

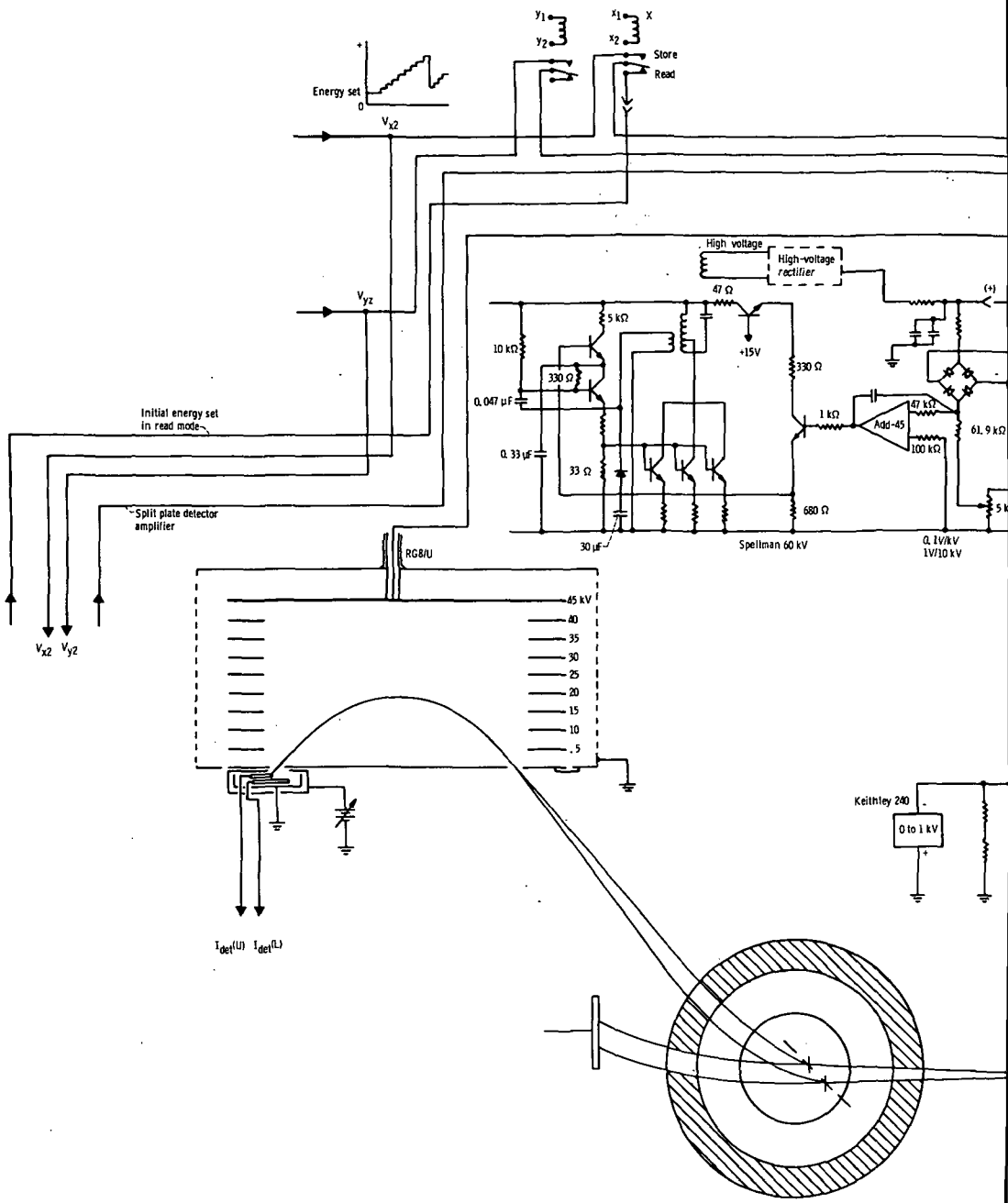

(b) Concluded.

Figure 6. - Concluded.

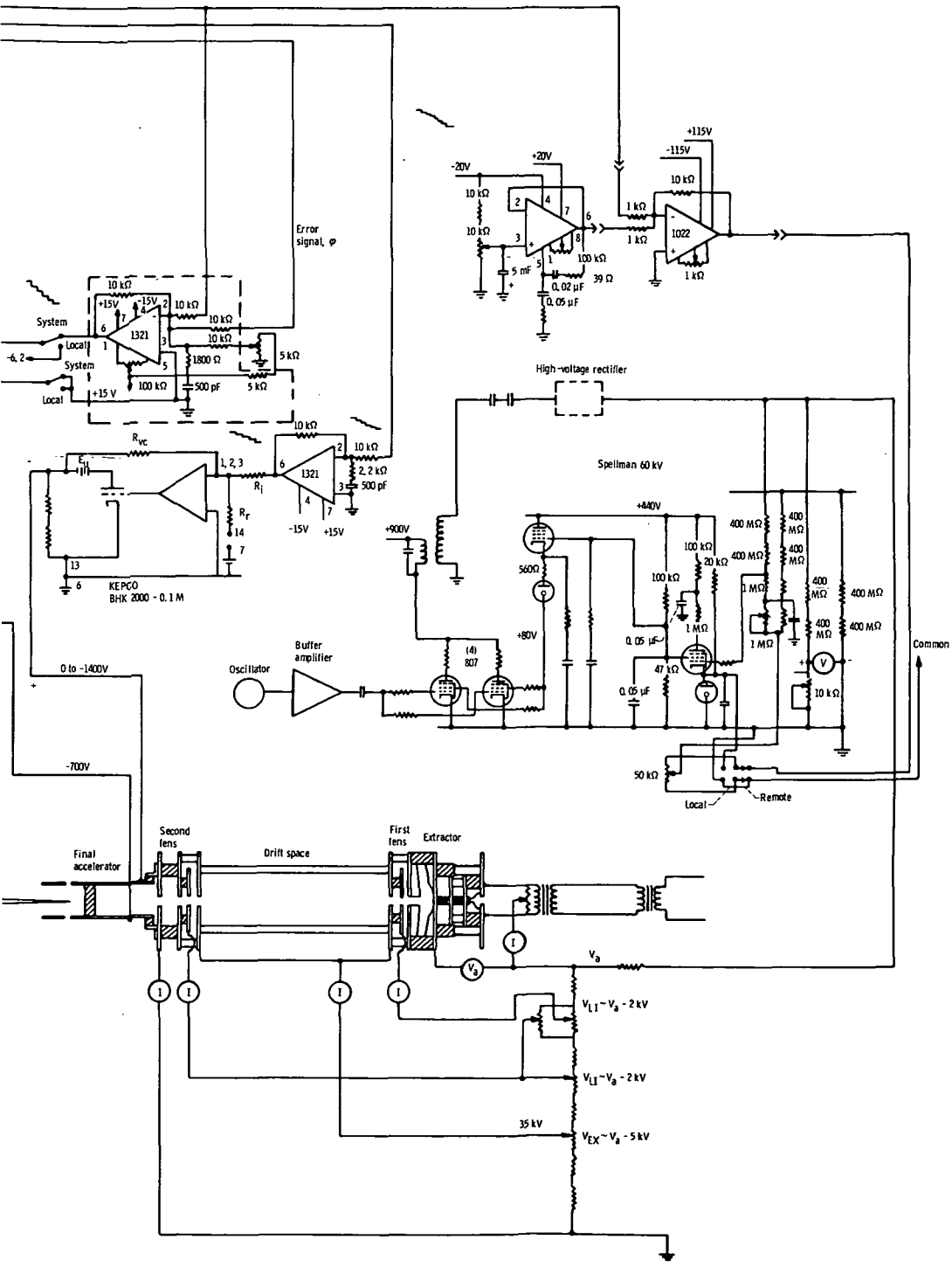
Error signal, φ
System
Local
-6.2
System
Local
+15 V
10 kΩ
1321
1800 Ω
5 kΩ
100 kΩ
500 pF
5 kΩ
R_{vc}
E_H
R_i
R_f
KEPCO
BHK 2000 - 0.1 M
2.2 kΩ
500 pF
-15V
+15V
-20V
+20V
5 mF
100 kΩ
0.02 μF
0.05 μF
39 Ω
+115V
-115V
1022
1 kΩ
High-voltage rectifier
Spellman 60 kV
+900V
+440V
560Ω
+80V
(4)
807
Buffer amplifier
Oscillator
0 to -1400V
-700V
400 MΩ
20 kΩ
1 MΩ
0.05 μF
47 kΩ
50 kΩ
Local
Remote
Common
Final accelerator
Second lens
Drift space
First lens
Extractor
V_a
$V_{L1} \sim V_a$ - 2 kV
$V_{L1} \sim V_a$ - 2 kV
35 kV
$V_{EX} \sim V_a$ - 5 kV

circuitry provides signals to a deflection step control that causes the energy across the ion gun resistive divider to change, thus changing the energy of the beam injected into the plasma. It also changes the voltage across the deflection plates of the ion gun, thus varying the injection angle of the primary beam into the plasma. Since varying the primary-beam energy and injection angle moves the ionization point around in the plasma, an array of points inside the plasma volume is sampled, each of which is an ionization point in the ideal case. The number of ionization points examined can be controlled by appropriate scaling of the scan control and by adjusting the increments in both energy and angle. The scan control also provides a signal to the power supply that drives the electrostatic analyzer.

The secondary ion beam results from the interaction of the plasma with the primary beam. The secondary beam enters the analyzer and is deflected into the split-plate detector, where the total current is measured. A detector amplifier measures the current and provides a signal to a feedback circuit that drives the analyzer power supply in order to keep the secondary beam focused on the split-plate detector. The voltage across the analyzer is varied until the current to each plate of the detector is equalized. Since the feedback signal to the analyzer is proportional to the difference in the energy of the primary ion beam as compared with the energy of the secondary beam, this feedback signal is a measure of the plasma potential. The total secondary-beam current, which is proportional to the electron density, can also be recorded. The feedback signal or the total secondary current signal is sent through a voltage-to-frequency converter and is then stored in an appropriate channel in a multichannel analyzer. The magnitude of each signal can be read out on the z-axis of an oscilloscope (intensity), while the x- and y-axes can be related to x- and y-positions inside the plasma. The data can also be printed or punched out for further computer analysis.

This control system is basic to any ion beam probing system that is used for time- or space-resolved plasma measurements. This particular system has not been used as a complete driving and feedback control system because of time limitation and an inadequate secondary-beam signal. The secondary signals are always less than 1 nanoampere and have usually been less than 100 picoamperes. These signals can be detected but are too small to be used in the present secondary-beam detector amplifier circuit. The electron density implied by the magnitude of these signals is approximately 10^{10} to 10^{11} per cubic centimeter. There is usually a unique secondary signal associated with each set of primary-beam initial conditions. However, for this plasma, we have found that more than one secondary beam can be observed in the electrostatic analyzer for one set of primary-beam conditions.

The expected current can be calculated from the relation between the primary and secondary ion beam currents:

$$\frac{I_{t2}}{I_{t1}} = 2N_e \frac{\langle \sigma v \rangle}{v_b} l \tag{5}$$

where I_{t1} and I_{t2} are the primary- and secondary-beam currents, respectively, v_b is the velocity of the beam ions, N_e is the electron density, and $\langle \sigma v \rangle / v_b$ is the effective cross section (ref. 5). The term $\langle \sigma v \rangle$ is obtained by averaging the cross section for ionization over an assumed Maxwellian electron distribution, and l is a resolution length of the electrostatic analyzer along the beam. For this example, a good estimate for l is 1 centimeter, which is obtained by varying the ionization point of the secondary beam and observing the effect at the electrostatic analyzer. The secondary currents would then be estimated as 10^{-5} to 10^{-3} microampere (using $I_{t1} = 0.5$ μA, $E_0 \cong 20$ keV, $\langle \sigma v \rangle / v_b \approx 10^{-14}$ cm^2 (ref. 5), at an estimated electron temperature of 100 eV).

COMPUTER CALCULATIONS

The modified Penning discharge has strong electric fields in the interior of the plasma. The computation must correctly locate the ionization point at which the observed secondary ions are being emitted. The location of the ionization point must be compatible with the ion beam initial conditions, the observed secondary ion energies, and the plasma space potential profile.

The calculation of a particle trajectory is a straightforward problem, which is found by solving equation (4). This is the equation of motion of a particle of mass m and charge q in electric and magnetic fields, E and B, respectively. The magnetic field is specified everywhere along the orbit. This is true for low-β plasmas, such as the modified Penning discharge where β is less than 10^{-4} (β is the ratio of plasma pressure to magnetic field pressure (ref. 16)). Also, the current density in the plasma must be low. In the modified Penning discharge, the total current is less than 1 ampere. A current along the magnetic field axis would create a poloidal field that would bend the beam out of the two-dimensional plane used to model this plasma. It is possible to measure the current density by using this deflection (refs. 17 and 18).

The computer program input consists of the primary-beam initial conditions and the model potential profile parameters. For the primary-beam trajectory calculation alone, this is enough information. The calculation of the best-fitting parameters can then proceed as described in reference 11. Calculating the secondary orbits is no more complex than calculating the primary orbits. The program picks points along the primary path where the charge of the ion is set equal to 2e. The actual ionization point in the plasma is unknown, but there is a large change in the secondary ion energy after it leaves the plasma. The program uses this to locate ionization points. The program searches for

the largest change in the secondary ion energy. Using the model potential, it attempts to match this energy with a particular measured secondary ion energy. It does this by continuing to vary the model parameters in an iterative loop.

The anode rings and grounded screen in the modified Penning discharge are concentric. It is convenient to assume circular symmetry for the model and to ignore effects due to the anode support shaft. With the symmetry assumption we can numerically solve for the vacuum field by using a program that solves Laplace's equation (ref. 19). This vacuum field is shown in figure 9 along with a plot of the assumed potential (ref. 8). It provides a first step to the model profile. When the plasma is present, the anode is

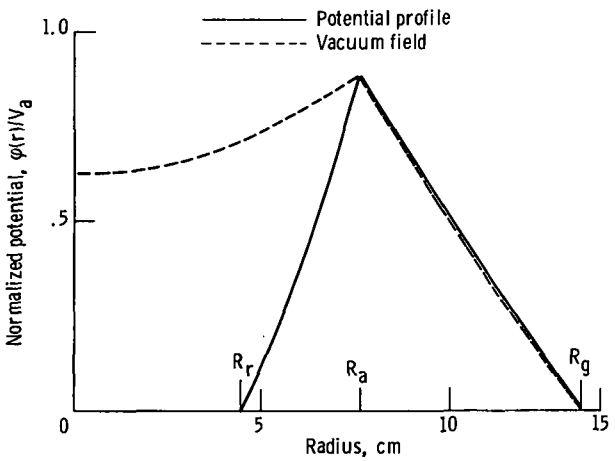

Figure 9. - Initial potential profile and vacuum field.

shielded within a Debye length, and the potential is expected to be less than the vacuum field inside the anode ring. Previous research on the discharge indicates a model for the shape of the potential inside the anode (ref. 8). The particular potential obtained is a function of r^2 and, if the potential is assumed never to be less than zero, it can be written in the form

$$\varphi = C_1 r^2 + C_2 \tag{6}$$

where $\varphi = 0$ when $r^2 = -C_0/C_1$. A potential of this type is assumed for the region inside the anode ring. We model the potential outside the anode by the vacuum field and inside by the function in equation (6). Dow (ref. 20) has suggested that there may be potentials greater than zero on the axis of a Penning discharge. The model can allow for this by scaling the potential in equation (6). Finally, a flat region is inserted near the peak potential. The resulting model is shown in figure 10. The five parameters are φ_{max}, φ_{in}, R_i, R_o, and R_r. In the region $R_g \geq r \geq R_i$, the potential is assumed to

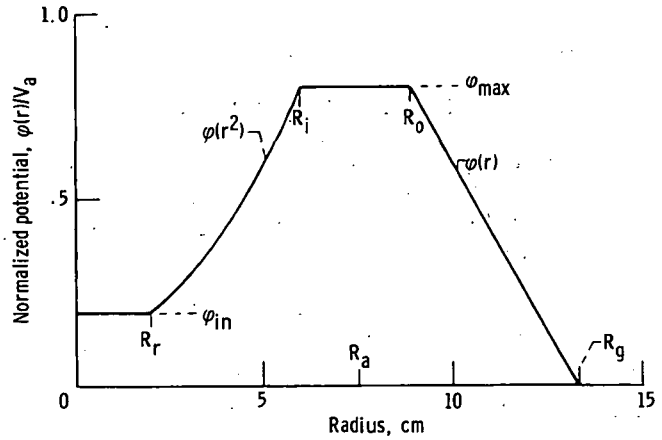

Figure 10. - Assumed model of potential profile.

be a linear function of r. As can be seen from the vacuum field solution in figure 9, this is a good approximation. The potential assumes the value φ_{max} in the region $R_o \geq r \geq R_i$. The potential is described by equation (6), and this equation is scaled depending on the value of φ_{in} in the region $R_i \geq r \geq R_r$. The potential would be divided into as many regions as needed to improve the fit of the final potential. The computations are one dimensional.

EXPERIMENTAL PROCEDURES

Experimental results obtained in this device have been reported elsewhere (ref. 11). A summary of the experimental methods and procedures is given here.

The primary beam was first examined with no plasma present. The results are given in table I. One important point of this table is that, for the single magnetic field strength used, a beam energy of about 6 keV was sufficient to deflect the primary beam into the electrostatic analyzer. It was found that a systematic error of about 1.50 degrees exists in the computation of the orbit. Estimates of the error in the location of the beam emission point caused the overall estimate of angular error to be about ±2 degrees. For these initial measurements, this was considered acceptable. Table II gives data on the primary-beam trajectories for various discharge conditions. Listed are the primary-beam energy, injection angle, and trajectory end point and the plasma discharge conditions. Beam angles varied from 43.3° to 35.3°. The plasma is characterized by the Penning anode voltage and the background deuterium pressure, which is measured with an ionization gage. The voltage ranges from 4.5 to 17 kilovolts, and the background neutral density from 2.8×10^{10} to 1.6×10^{12} neutral particles per cubic centimeter. The best parameters, in terms of obtaining usable experimental data, were an

TABLE I. - TYPICAL MEASURED AND CALCULATED PRIMARY-ION-BEAM TRAJECTORIES WITH DISCHARGE TURNED OFF

Primary beam		End point		Type of result, measured (M) or calculated (C)
Energy, keV	Injection angle, deg	Radius, r, cm	Angle, $\theta + 0.5^{\circ}$, deg	
6.15	39.8	92.5	1.6	M
6.1	39.5	↓	.8	C
6.1	40		1.0	↓
6.2	39.5		1.1	
6.2	40	↓	1.3	
20	41	42.7	25.4	M
20	41	↓	26.6	C
22	42.2		25.4	M
22	42		24.5	C
22	42.5		24.6	C
17.8	42.5		25.4	M
17.8	42.5		22.2	C
31.8	39.5		22.4	M
31.8	39.5		20.3	C
18	43.1		25.4	M
18	43.1	↓	22.4	C

anode voltage V_a of approximately 10 kilovolts and a background neutral density of 4.5×10^{11} to 5.5×10^{11} neutral particles per cubic centimeter. Problems encountered under other conditions are discussed in the next section.

Table II points up some unique problems of probing a high-voltage plasma discharge with an ion beam. For low discharge voltages (~5 kV) the trajectories are governed primarily by the magnetic field. Examples of this are beam energies E_i of 19.8 and 30.6 keV in table II. For plasma operating conditions of $1.7\times10^{10}/cm^3 \leq N_o \leq 5.5\times10^{11}/cm^3$ (0.5×10^{-6} torr $\leq P \leq 16\times10^{-6}$ torr) and anode voltages above 5 kilovolts, the effects of the electric field became apparent. For energies between 11.5 and 22.0 keV, the beam was deflected through an angle of 39.3°, in order to be observed in the electrostatic analyzer. A beam deflection much less than 39.3° could be seen on the primary detector. A plot of a trajectory of these beams shows that the electrostatic field was changing the curvature of the orbit due to the magnetic field, as illustrated in figure 11.

The experimental results given in table II were examined by using an orbit computation program with an assumed potential profile. An initial estimate of the radial

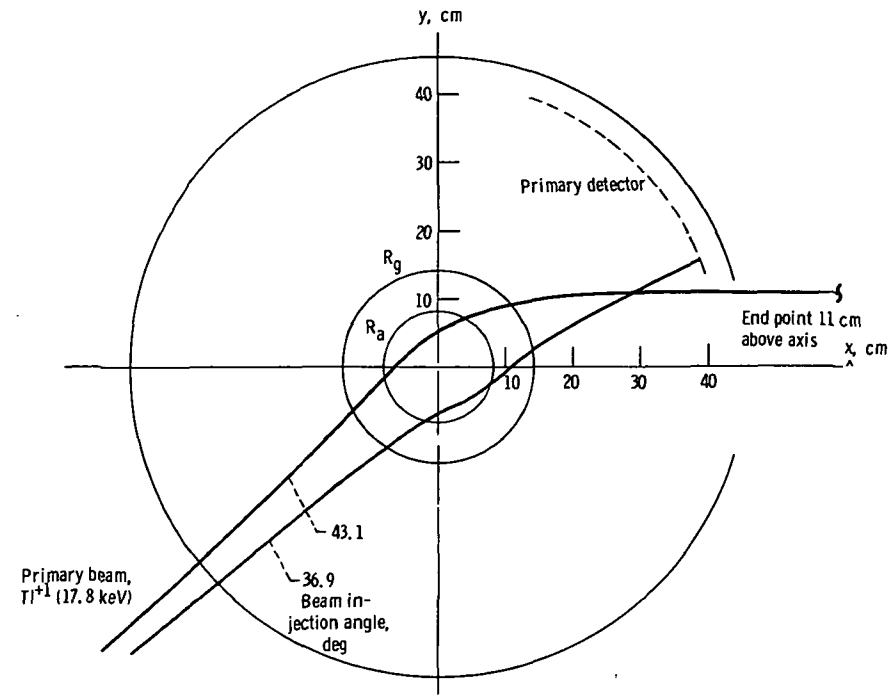

(a) Case 1 (table III). Measured trajectories for beam injection angles of 43.1° (electrostatic analyzer) and 36.9° (for end point of 42.7-cm radius and 22.4°). Calculated trajectories for beam injection angles of 43.1° and 36.9° (for end point of 42.7-cm radius and 22.2°).

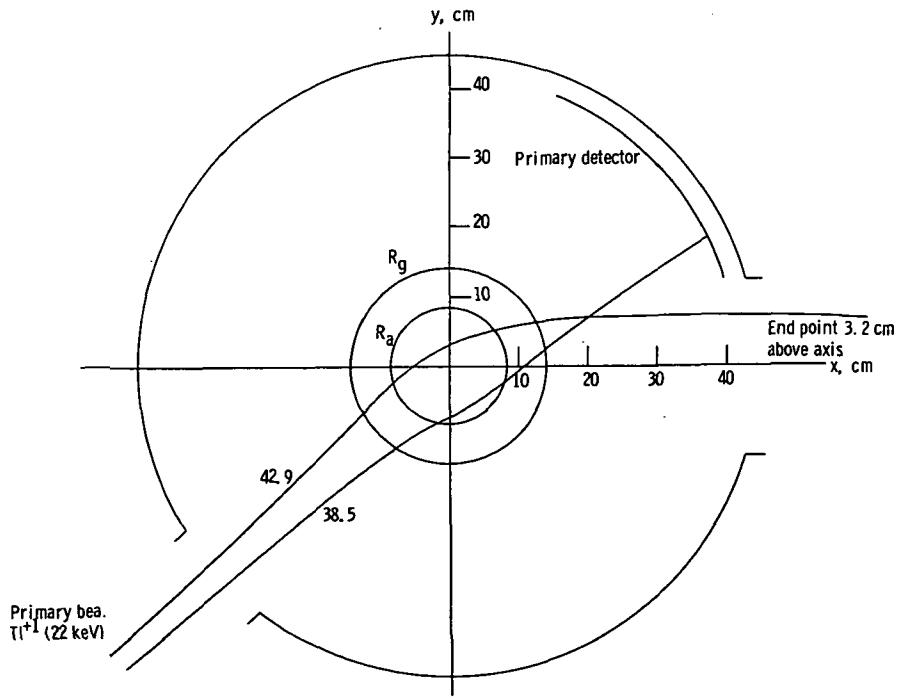

(b) Case 2 (table III). Measured trajectories for beam injection angles of 42.9° (electrostatic analyzer) and 38.5° (for end point of 42.7 cm and 25.4°). Calculated trajectories for beam injection angles of 42.9° and 38.5° (for end point of 42.7 cm and 25.1°).

Figure 11. - Calculated trajectories for model potentials.

TABLE II. - EXPERIMENTAL PRIMARY-ION-BEAM INITIAL CONDITIONS AND END POINTS FOR VARIOUS PLASMA OPERATING CONDITIONS

Primary beam		End point		Plasma		
Energy, keV	Injection angle, deg	Radius, r, cm	Angle, $\theta + 0.5^{\circ}$, deg	Anode voltage, V_a, kV	Pressure, P	
					Neutral particles per cm^3	torr
17.8	36.9	42.7	22.4	10.4	5.5×10^{11}	15.9×10^{-6}
17.8	43.1	92.5	1.6	10.4	5.5	15.9
22.0	38.5	42.7	25.4	13.2	2.8×10^{10}	.8
22.0	42.9	42.5	1.6	13.2	2.8	.8
17.6	36.9	42.7	22.4	10	5.5×10^{11}	15.9
17.6	43	92.5	1.6	10	5.5	15.9
17.3	38.3	42.7	22.4	10.1	1.7×10^{10}	.5
17.3	43.1	92.5	1.6	10.1	1.7	.5
11.5	36	42.7	22.4	6	5.5×10^{11}	15.9
11.5	42.6	92.5	1.6	6	5.5	15.9
31.7	39.3	42.7	22.4	10	5.5	15.9
18	37.7	42.7	25.4	9.4	4.6	13.25
24.5	36.9	42.7	25.4	13.2	2.8×10^{10}	.8
23.6	42.9	92.5	1.6	17	4.6×10^{11}	13.25
23.1	37.6	42.7	20.9	7.5	↓	↓
12.5	34.7	42.7	25.4	5.8		
16	47.86	92.5	1.6	12		
18	35.4	42.7	20.9	10		
18	35.2	42.7	22.4	10		
19.4	41.7	92.5	1.6	9.8		
19.8	44.3	42.7	22.4	4.5		
19.1	36.8	42.7	22.4	10	4.7	13.5
20.3	41	92.5	1.6	11.2	4.6	13.25
20.3	36.7	42.7	25.4	11.2	↓	↓
30	38.6	↓	20.9	11.2		
30.6	42.7		25.4	5.3		
37.2	38.9		22.4	5.4	9.1×10^{10}	2.65
31.6	41.1		26.8	5	1.8	53

electrostatic potential is used in the program. The parameters shown in figure 10 divide the radial potential profile into four regions. The vacuum field is a computed solution of Laplace's equation in cylindrical symmetry, which is assumed for the modified Penning discharge. Inside the radius R_i, the model potential is proportional to r^2 plus a constant, which gives an electric field proportional to r in this region (ref. 8).

To optimize the model parameters, a minimization calculation is carried out, with the quantity M defined as

$$M = \sum_{i=1}^{n} (\theta_{mi} - \theta_{ci})^2 \qquad n = 1, 2, \ldots \tag{7}$$

where the angles in this expression are the coordinates of the trajectory at the detector and θ_{mi} and θ_{ci} are from the measured and calculated beams, respectively. The

calculated angles are a function of the five parameters (R_i, R_o, R_r, φ_{max}, and φ_{in}). The minimization involved a choice of an initial estimate and the iterative variation of the five parameters. The order of variation was φ_{max}, R_r, φ_{in}, R_i, and R_o. The initial estimate is shown in figure 11 and is consistent both with the vacuum field solution for $r \geq R_o = R_a$ and with the discussion of reference 8 for $R_r \leq r \leq R_i = R_a$. The primary-beam initial conditions and trajectory are taken from the first two columns in table III. The initial estimate for the two cases examined in detail is specified by $R_i = R_o = R_a$, $R_r/R_a \cong 0.87$, $\varphi_{in} = 0$, and $\varphi_{max} \simeq 0.88\ V_a$. The iteration processes used are described in reference 11. The results of the calculation are given in figure 12

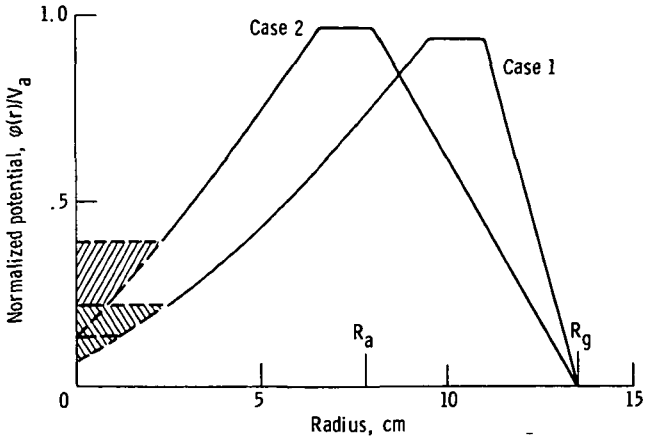

Figure 12. - Potential profiles for cases 1 and 2 (table III), obtained by minimization of the parameter M (eq. (7)).

as radial potential profiles. The characteristics of the potentials are (1) V_{max} is close to V_a and (2) there are nonzero potentials on the discharge axis. The result that $R_i > R_a$ is corroborated by two pieces of evidence: (1) the location of $R_i/R_a > 1$ and $R_o/R_a > R_i/R_a$ minimizes M, and (2) this potential predicts multiple secondary energies that are observed in the experiment. Within experimental error, the potentials in the modified Penning discharge are a maximum close to the anode voltage and nonzero on the axis.

Unless the ion orbits cross the discharge axis, we cannot have direct knowledge of the region inside the distance of closest approach to the plasma center. The profiles in figure 12 were used to predict secondary-ion trajectories from points along the primary-ion beam. The result was that under some plasma conditions (e.g., those in case 1 in table III) multiple secondary-ion beams are created and can be detected in the electrostatic analyzer. The potential from case 1 of figure 12 was used in this calculation. The energy of the primary ions is specified. If the potential is that given in figure 12, secondaries emitted from the primary beam at three points in the plasma

TABLE III. - COMPARISON OF CALCULATED AND MEASURED

END POINTS FOR TWO DISCHARGE CONDITIONS

Case	Primary beam		End point		Type of result, measured (M) or calculated (C)	Plasma		
	Energy, keV	Injection angle, deg	Radius, r, cm	Angle, θ, deg		Anode voltage, V_a, kV	Pressure, P	
							N/m^2	torr
1	17.8	36.9	42.7	22.4	M	10.4	55×10^{10}	15.9×10^{-6}
			42.7	22.2	C			
		43.1	92.5	1.6	M	10.4	55	15.9
			92.5	8.9	C			
2	22.0	38.5	42.7	25.4	M	13.2	2.8×10^{10}	0.8×10^{-6}
			42.7	25.1	C			
		42.9	92.5	1.6	M	13.2	2.8	0.8
			92.5	3.9	C			

would enter the electrostatic analyzer. The energies and the emission points are specified in table IV and are also shown in figure 13. Such peaks were observed experimentally for the primary beam and plasma conditions listed in figure 13. Table IV and figure 13 show that we have established a possible potential for the plasma. The primary beam is observed in the electrostatic analyzer as predicted by the computer. Additional adjustment of the model potential profile is required to minimize the difference ($\approx$10 percent) between calculated and measured orbits for the secondaries.

TABLE IV. - CALCULATED SECONDARY-

ION-BEAM TRAJECTORIES AND

ENERGIES FROM CASE 1 OF

TABLE III AND COMPARISON

WITH EXPERIMENT

Calculated energies, keV	Calculated ionization point, (x, y), cm	Measured energies, keV
25	-9.2, -6.0	23
27	-8.2, -5.0	26.5
22	5.2, 3.0	19.8

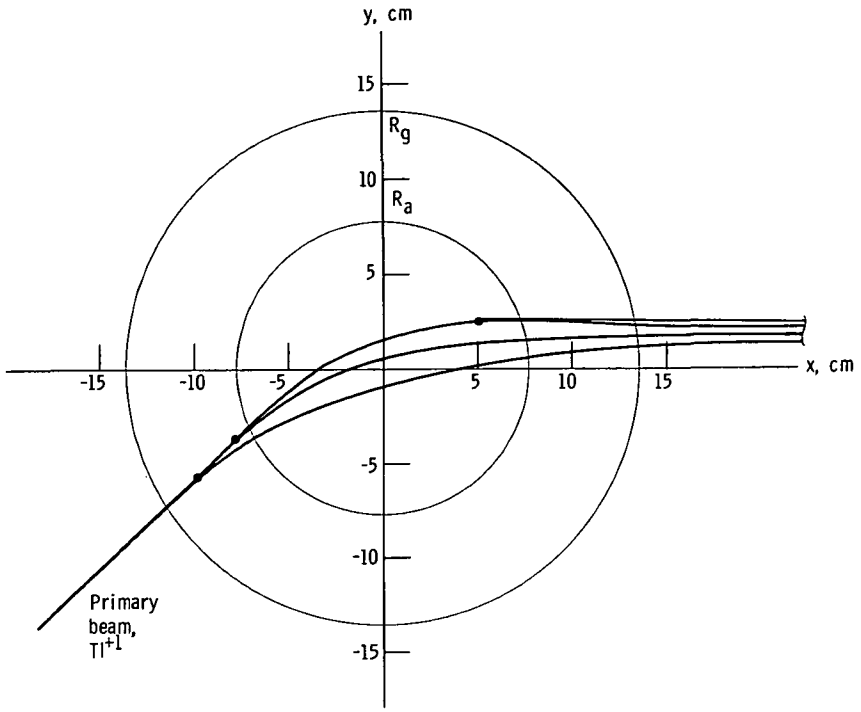

Figure 13. - Predicted secondary-beam paths for case 1 (ta.

DEVELOPMENTAL PROBLEMS

High-voltage breakdown is a problem when the plasma being probed emits energetic particles and radiation. The modified Penning discharge produces hot ions, ultraviolet rays, and soft X-rays. The hot ions produce noise in the electrostatic analyzer. Depending on the discharge background pressure and the anode voltage, a signal may be received in the analyzer with the ion gun off. These ions originate in the plasma. Since they are most probably D^+ or D_2^+, they are observed in the analyzer at voltages numerically equal in volts to twice the ion energy in electron volts. Hence, a 10-keV ion would be observed at 20 kilovolts. These ion energies are equal to or slightly less than the anode voltage. The intercepted current in the analyzer from these plasma ions is large enough to mask the secondary current from the ion probing beam. A simple sector magnet or a second set of electrostatic deflector plates was used to filter out these plasma ions.

The flow of background plasma into the electrostatic analyzer and the ion gun must be kept to a minimum, for example, by differentially pumping the gun and analyzer regions. If the system is not differentially pumped, careful attention must be given to baffling and shielding. In this mirror machine, the plasma flows out the ends of the magnetic bottle, and a weak background plasma may exist near the gun and the analyzer. This problem may be unique to this experiment because the magnets and the Penning

discharge are contained in a single large vacuum tank.

In this experiment, the ion gun was run without differential pumping. The range of the accelerating voltage on the gun was 6 to 40 kilovolts. The background neutral gas density in the discharge was 4×10^{9} to 1.7×10^{12} neutral particles per cubic centimeter. An optical baffle was placed in the path of the beam to the plasma with a small opening for the primary beam. This eliminated radiation as an ionizing mechanism in the ion-gun bell jar. However, even with an optical baffle and metal screening in the pumping path between the ion gun and the vacuum tank, a weak plasma continued to diffuse into the gun bell jar. This usually occurred at background neutral gas densities of 8.6×10^{11} neutral particles per cubic centimeter and anode voltages above 10 kilovolts. This weak plasma caused continuous arc discharges in the region of the gun. These discharges were reduced in intensity or disappeared as the discharge pressure, the anode voltage, or the gun accelerating voltage was reduced.

The level of secondary signal strength in the plasma of interest should also be examined. Estimates of the maximum density obtainable in this plasma are 10^{9} to 10^{11} electrons per cubic centimeter at maximum density conditions. These densities are less than those seen in previous ion beam probe work, in which nanoamperes of secondary current were detected for microamperes of primary current in plasmas where the densities were 10^{11} to 10^{13} electrons per cubic centimeter (refs. 1, 15, and 21). Here, we expect to see secondary currents 1 to 100 times smaller than those seen in previous work. Such currents were detected but only by nonautomatic operation of the probe.

In an effort to understand more about the potential profile in the modified Penning discharge, we used an actuated Langmuir probe assembly to examine the region along a radial line through the midplane between the electrode rings. The results are shown in figure 14. The magnitudes of the measured profiles are neither those expected from the vacuum field solution nor those obtained from the computer modeling procedure. Results were obtained to within 3 millimeters of the anode, and the measured probe voltage was never greater than $0.4\ V_a$ and varied with pressure. The probe could not measure the potential at the lowest discharge pressure, less than 4×10^{9} electrons per cubic centimeter. Primary-beam orbits calculated from these potentials in the computer program were not in agreement with those measured. The ion beam results are considered to be more reliable than the Langmuir probe results, since the latter apparently disturbed the plasma to such an extent that profiles consistent with other data could not be obtained.

The experimental results from this device are valuable in that they verify a particular model of the discharge. The interpretation of the results is model dependent, but we think that the general characteristics of the size and shape of the potential would result no matter what initial model was chosen, as long as the boundary conditions of

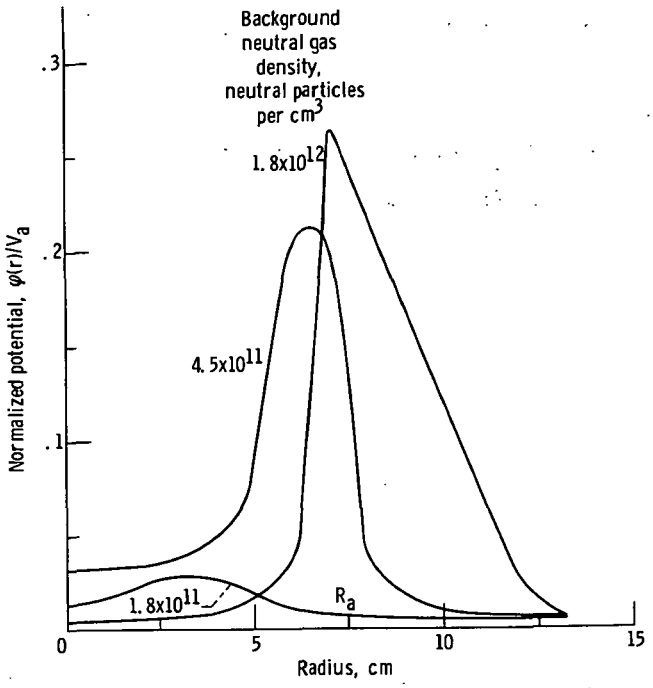

Figure 14. - Potential measured with Langmuir probe in anode ring midplane.

the modified Penning discharge were taken into account. Secondary beams have been observed, and a more extensive model with more parameters can be constructed. Since the model would have to describe the primary and all the secondary trajectories that were observed, confidence in the final model results would be increased.

CONCLUSIONS

It is possible to do ion beam probing of a plasma, the floating potentials of which are comparable in magnitude to the energy of the probing ion beam, and to obtain radial time-averaged potential profiles. The presence of large floating potentials in the plasma makes it necessary to use an iterative computer program to interpret data provided by the primary and secondary ion beams. Several examples were observed for which the computer-derived radial potential profile correctly predicted the energy and momentum of both the primary and secondary ion beams. The experience obtained in developing mechanical and electronic components to probe plasma potentials comparable to the primary-beam energy has been documented. This experience may be useful

in developing advanced ion beam probing systems for fusion-related plasmas which have strong electric fields or which contain high floating potentials.

Lewis Research Center,
National Aeronautics and Space Administration,
Cleveland, Ohio, October 1, 1976,
506-25.

APPENDIX - SYMBOLS

B	magnetic field
C_1, C_2	constants in assumed potential profile (eq. (6))
E	electric field
E_i	ion energy along beam path
E_0	initial ion energy
e	electronic charge
I_{t1}, I_{t2}	primary and secondary beam currents
l	resolution length of electrostatic analyzer
M	minimization parameter (eq. (7))
m	mass of particle
N_e	electron density
N_0	background neutral gas density
P	pressure
q	charge of particle
R_a	anode radius
R_g	radius of grounded boundary
R_i	inner radius of potential maximum
R_o	outer radius of potential maximum
R_r	outer radius of potential minimum
r	radius
s	length along beam path
V_a	anode voltage
V_{ea}	voltage across analyzer
V_{max}	maximum potential
v_b	velocity of beam ions
θ_{ci}	calculated trajectory angle
θ_{mi}	estimated trajectory angle
$\langle\sigma v\rangle/v_b$	effective cross section

φ	potential
φ_{in}	minimum potential along plasma radius
φ_{max}	maximum potential along plasma radius
φ_s	space potential along beam path

REFERENCES

1. Jobes, F. C.; Marshall, J. F.; and Hickok, R. L.: Plasma Density Measurement by Ion-Beam Probing. Phys. Rev. Lett., vol. 22, no. 20, May 19, 1969, pp. 1042-1045.

2. Jobes, F. C.; and Hickok, R. L.: A Direct Measurement of Plasma Space Potential. Nucl. Fusion, vol. 10, no. 2, June 1970, pp. 195-197.

3. Hickok, R. L.; Reinovsky, R. E.; and Jennings, W. C.: Beam Probe Systems for Future CTR Devices. Bull. Am. Phys. Soc., vol. 18, no. 10, Oct. 1973, pp. 1277.

4. Hickok, R. L.; Jobes, F. C.; and Marshall, J. F.: Beam Probe Mapping of Rapidly Fluctuating Plasma Density in an Energetic Arc. AFOSR-69-0644TR; FR-4, Mobil Research and Development Corp., 1969.

5. Hickok, Robert L.; and Jobes, Forrest C.: Heavy-Ion Beam-Probe Systems for Plasma Diagnostics. AFOSR-70-2354TR; FR-5, Mobil Research and Development Corp., 1970.

6. Jobes, F. C.; Hosea, J. C.; and Hickok, R. L.: Preliminary Ion Beam Measurement of the Current Distribution in the ST Tokamak. Bull. Am. Phys. Soc., vol. 17, no. 11, Nov. 1972, pp. 984.

7. Roth, J. Reece; Freeman, Donald C., Jr.; and Haid, David A.: Superconducting Magnet Facility for Plasma Physics Research. Rev. Sci. Instrum., vol. 36, no. 10, Oct. 1965, pp. 1481-1485.

8. Roth, J. R.: Hot Ion Production in a Modified Penning Discharge. IEEE Trans. Plasma Sci., vol. PS-1, no. 1, Mar. 1973, pp. 34-45.

9. Roth, J. Reece; et al.: Performance of a 12-Coil Superconducting "Bumpy Torus" Magnet Facility. Presented at Symposium on the Technology of Controlled Thermonuclear Fusion Experiments and the Engineering Aspects of Fusion Reactors, Nov. 1972.

10. Roth, J. Reece; Richardson, Richard W.; and Gerdin, Glenn A.: Initial Results from the NASA Lewis Bumpy Torus Experiment. NASA TM X-71468, 1973.

11. Kambic, George X.: Heavy Ion Beam Probe Measurements of Radial Potential Profile in the Modified Penning Discharge. NASA TM X-71643, 1974.

12. Pierce, John R.: Theory and Design of Electron Beams. Second ed., Van Nostrand, 1954.

13. Hickok, Robert L.; and Jobes, Forrest C.: Ion Beam Probe for ST Tokamak. AFOSR-72-0018TR; SR-6, Mobil Research and Development Corp., 1972.

14. Green, T. S.; and Proca, G. A.: A Parallel Plate Electrostatic Spectrograph. Rev. Sci. Instrum., vol. 41, no. 10, Oct. 1970, pp. 1409-1414.

15. Reinovsky, Robert E.: An Ion Beam Probe Diagnostic Technique for Laboratory Plasmas. Ph. D. Thesis, Rensselaer Polytechnic Inst., 1973 (see also RPDL-73-13; AFOSR-74-0242TR).

16. McNeilly, G. S.: Heavy-Ion Beam Design Calculations for the ORMAK and ELMO Bumpy Torus Devices. ORNL-4834, Oak Ridge National Lab., 1973.

17. Hickok, R. L.; et al.: Ion Beam Probe Diagnostic System. COO-2229-2, Rensselaer Polytechnic Inst., 1973.

18. Hickok, R. L.; Huchital, G. S.; and Jobes, F. C.: Extraction of J from Ion Beam Measurements on ST. Bull. Am. Phys. Soc., vol. 17, no. 11, Nov. 1972, p. 984.

19. Bogart, Carl D.; and Richley, Edward A.: A Space-Charge-Flow Computer Program. NASA TN D-3394, 1966.

20. Dow, D. G.: Electron-Beam Probing of a Penning Discharge. J. Appl. Phys., vol. 34, no. 8, Aug. 1963, pp. 2395-2400.

21. Hosea, J. C.; et al.: Rotation and Structure of Low-Frequency Oscillations inside the ST-Tokamak Plasma. Phys. Rev. Lett., vol. 30, no. 18, Apr. 30, 1973, pp. 839-842.

NATIONAL AERONAUTICS AND SPACE ADMINISTRATION
WASHINGTON, D.C. 20546

OFFICIAL BUSINESS
PENALTY FOR PRIVATE USE $300

SPECIAL FOURTH-CLASS RATE
BOOK

POSTAGE AND FEES PAID
NATIONAL AERONAUTICS AND
SPACE ADMINISTRATION
451

U.S.MAIL

POSTMASTER : If Undeliverable (Section 158 Postal Manual) Do Not Return

"The aeronautical and space activities of the United States shall be conducted so as to contribute . . . to the expansion of human knowledge of phenomena in the atmosphere and space. The Administration shall provide for the widest practicable and appropriate dissemination of information concerning its activities and the results thereof."

—NATIONAL AERONAUTICS AND SPACE ACT OF 1958

NASA SCIENTIFIC AND TECHNICAL PUBLICATIONS

TECHNICAL REPORTS: Scientific and technical information considered important, complete, and a lasting contribution to existing knowledge.

TECHNICAL NOTES: Information less broad in scope but nevertheless of importance as a contribution to existing knowledge.

TECHNICAL MEMORANDUMS: Information receiving limited distribution because of preliminary data, security classification, or other reasons. Also includes conference proceedings with either limited or unlimited distribution.

CONTRACTOR REPORTS: Scientific and technical information generated under a NASA contract or grant and considered an important contribution to existing knowledge.

TECHNICAL TRANSLATIONS: Information published in a foreign language considered to merit NASA distribution in English.

SPECIAL PUBLICATIONS: Information derived from or of value to NASA activities. Publications include final reports of major projects, monographs, data compilations, handbooks, sourcebooks, and special bibliographies.

TECHNOLOGY UTILIZATION PUBLICATIONS: Information on technology used by NASA that may be of particular interest in commercial and other non-aerospace applications. Publications include Tech Briefs, Technology Utilization Reports and Technology Surveys.

Details on the availability of these publications may be obtained from:

SCIENTIFIC AND TECHNICAL INFORMATION OFFICE

NATIONAL AERONAUTICS AND SPACE ADMINISTRATION

Washington, D.C. 20546